Journal of Computational Physics 282 (2015) 317–333

Contents lists available at ScienceDirect

Journal of Computational Physics

www.elsevier.com/locate/jcp

A new non-overlapping concept to improve the Hybrid Particle Level Set method in multi-phase fluid flows

Philip J. Archer, Wei Bai *

Department of Civil and Environmental Engineering, National University of Singapore, 1 Engineering Drive 2, Singapore 117576, Singapore

ARTICLE INFO

Article history:
Received 30 October 2013
Received in revised form 26 August 2014
Accepted 17 November 2014
Available online 25 November 2014

Keywords:
Level set method
Particle correction
New reseeding algorithm
Non-overlapping concept
Multi-phase flow

ABSTRACT

A novel non-overlapping concept is augmented to the Hybrid Particle Level Set (HPLS) method to improve its accuracy and suitability for the modelling of multi-phase fluid flows. The concept addresses shortcomings in the reseeding algorithm, which maintains resolution of the surface at runtime. These shortcomings result in the misplacement of newly seeded particles in the opposite signed domain and necessitate a restriction on the distance that a particle can escape without deletion, which reduces the effectiveness of the method. The non-overlapping concept judges the suitability of potential new particles based on information already contained within the particle representation of the surface. By preventing the misplacement of particles it is possible to significantly relax the distance restriction thereby increasing the accuracy of the HPLS method in multi-phase flows. To demonstrate its robustness and efficiency, the concept is examined with a number of challenging test cases, including both level-set-only simulations and two-phase fluid flows.

1. Introduction

A better knowledge of the physics of breaking waves is fundamental to improving the design of structures to cope with the demands of the ocean environment. However, this subject presents many difficulties to traditional free surface modelling techniques. The numerical technique that is able to predict the position of the interface that separates the gas and liquid phases must allow for extreme surface curvature, entrainment of air, splitting and merging to make it applicable for complicated engineering and geophysical flows such as wave breaking, sloshing and bubble flows. Two different types of methods have been used extensively to account for a free surface in numerical simulations, namely surface tracking and surface capturing. In surface tracking techniques the interface grid is updated at each time step to coincide with the position of the surface boundary, such as in Tryggvason et al. [23]. Although very accurate for simple surface configurations, their limitation is in their inability to handle complex geometry and breaking waves.

Surface capturing techniques use a stationary computational grid with the interface defined implicitly after the solutions of the domain are obtained. The most popular methods of surface capturing are Marker-And-Cell (MAC), Volume-Of-Fluid (VOF) and the level set method. The MAC scheme introduces massless particles on the surface whose motion is tracked to reveal the transient surface boundary. Complicated surface geometries and wave breaking can be captured by this method. However, drawbacks of the method include the computational effort required to track the large number of Lagrangian particles and the smoothness of the resultant surface that is reconstructed from the particle locations. Recently, the VOF

* Corresponding author.
E-mail address: w.bai@nus.edu.sg (W. Bai).

http://dx.doi.org/10.1016/j.jcp.2014.11.018
0021-9991/

technique has become popular due in part to its excellent conservation properties, as undertaken by Kim et al. [12], Liu and Lin [14], Khezzar et al. [10] in the study of water sloshing. Another surface capturing technique which has recently gained great popularity in the simulation of multi-phase fluid flows is the Level Set Method (LSM), in which a scalar 'Level Set' function is defined throughout the domain. The magnitude of the level set function measures the distance from a point to the surface. A distinct advantage of the LSM is the simplicity with which surface curvature is represented, aiding the modelling of surface tension, and the ease of its implementation, see Osher and Fedkiw [17] for a review.

The major drawback of using the level set method is that it becomes inaccurate when the surface geometry is under-resolved, i.e. when the surface curvature is high. Error in the position of the zero level set (i.e. surface interface) violates the conservation of mass. One way in which the conservation can be guaranteed is by solution of a separate criteria that enforces mass conservation on a cell by cell basis. For example, a mass correction factor was incorporated by Yap et al. [27] who considered two immiscible fluids in a channel thus dropping the surface tension term from the Navier–Stokes equations. Yue et al. [28] also used a volume constraint when reinitialisating the level set function to conserve the volume of the fluids and Sussman and Puckett [22] coupled the level set method with the volume of fluid method. Although conservation of the global fluid mass is explicitly guaranteed it is not clear that the mass that is added to each cell is exactly the mass that was lost and is a potential source of error. Recently, Wang et al. [25] developed a new volume constraint, which treats neighbouring bubbles or droplets as a group so long as the spacing is less than three grid cells. The mass of the group is conserved rather than the individual member aiding the algorithm to handle splitting and merging of fluid.

An alternative method was proposed by Enright et al. [4], in which massless marker particles were used to better define the position of the interface. Known as the Hybrid Particle Level Set method (HPLS herein) the conservation improvement is made through correction of the grid based level set function by the Lagrangian particles. Since the particles follow the flow field characteristics they more accurately trace surface movement than the implicit calculation of the level set function. The HPLS method has been shown to perform particularly well for cases in which an arbitrary level set distribution is stretched in a prescribed velocity field to the point at which the width of level set function is of order the grid spacing. Whereas the standard level set solution loses significant fluid mass and volume conserving level sets introduce errors in the position of the interface, the HPLS method is extremely accurate to within a fraction of a percent. Later, Enright et al. [5] showed that the computational efficiency of the HPLS technique could be improved through the use of lower order schemes for both the advection of the level set function and time integration of the particles. Their test cases showed only a small decrease in the accuracy of the representation of the zero level set interface when compared to the standard HPLS.

However, the benefit of the HPLS method can be reduced when resolving unsteady multi-phase flows. If the surface is highly stretched for example in the case of oceanic breaking waves or violent sloshing in LNG tanks, the HPLS method in its standard form can degrade the solution necessitating the introduction of an additional restriction. This restriction enforces the deletion of particles that move across the surface into the opposite domain by a distance equal to 1.5 times their radius [6]. Whilst this restriction smooths and stabilises the surface through the removal of spurious particles, it also discards valuable information from valid particles thereby degrading the simulation. Wang et al. [24] attempted to address these issues by improving the particle correction procedure, although this improves mass conservation in simulations involving bubbles and droplets, a restriction is still required to simulate breaking waves and overturning fluid [1].

Here we seek to develop an improved HPLS technique in which the restriction can be relaxed or at best removed altogether. We accomplish this by first diagnosing the key flaws in existing particle level set methods and then propose routines to combat these issues. In the new approach we introduce a novel non-overlapping concept that effectively prevents the misplacement of new particles during the reseeding procedure. Our new algorithm has proved robust and enhances the mass conservation properties of our level set method which increases as the grids are refined allowing finer and finer flow features to be captured.

We first present a discussion on the particle level set method in the context of a two-dimensional constrained vortex flow. The limitation of the conventional HPLS methods is clearly shown through this example, however, the new improved HPLS method proposed here seems to provide almost perfect results. Strictly speaking, our method patches the flaw that exists in the latest HPLS technique, no matter how visible the improvement in the results is. The increase of conservation properties is further examined by a three-dimensional deformation flow and a bubble flow. Through the classical dam break case, we also investigate the influence of various parameters that are relevant to the improved HPLS method, and recommendations are made based on the comparison. With these recommended parameters, we finally study the impulsive sloshing, by which the capacity of the new HPLS method in accurately simulating complicated multi-phase fluid flows is demonstrated.

2. Mathematical model

In this study we investigate the motion of two incompressible fluids and capture the movement of the dividing interface (or free surface) by the Level Set Method (LSM). In LSM an additional scalar ϕ, known as the level set function, is specified throughout the domain representing the location of each grid cell relative to the free surface. Here, we define ϕ to be a signed distance function, which measures the shortest distance from the grid cell to the free surface (i.e. $|\nabla\phi| = 1$) and is positive in one fluid phase and negative in the other. Hence the free surface is colocated with the zero interface and is implicitly defined by the level set value at the surrounding grid nodes. The level set function is advected by the local velocity field according to

$$\frac{\partial \phi}{\partial t} + u_i \frac{\partial \phi}{\partial x_i} = 0, \tag{1}$$

where t is time, $u_i = (u, v, w)$ is the fluid velocity and $x_i = (x, y, z)$ is the spatial coordinate.

The motion of the two fluids is governed by the Navier–Stokes equations,

$$\frac{\partial u_i}{\partial t} + u_j \frac{\partial u_i}{\partial x_j} = \frac{1}{\rho(\phi)}\left(-\frac{\partial p}{\partial x_i} + \frac{\partial \tau_{ij}}{\partial x_j}\right) - \frac{1}{\rho(\phi)}\kappa(\phi)\sigma\delta(\phi)N_i(\phi) + f_i, \tag{2}$$

and the continuity equation,

$$\frac{\partial u_i}{\partial x_i} = 0, \tag{3}$$

where f_i represents body forces (which in our simulations is the gravitational acceleration g), ρ is the fluid density, κ denotes the surface curvature, σ is the surface-tension coefficient, δ is a smoothed delta function which is non-zero near to the free surface, N_i is the unit normal vector, p is the pressure and τ_{ij} are the viscous stress components given by

$$\tau_{ij} = \mu(\phi)\left(\frac{\partial u_i}{\partial x_j} + \frac{\partial u_j}{\partial x_i}\right), \tag{4}$$

where μ is the fluid viscosity. Both ρ and μ vary dependant on the local fluid phase properties and are smoothed across the free surface by use of a Heaviside function to avoid numerical instabilities caused by the sharp gradients present. We calculate ρ and μ by

$$\rho(\phi) = \rho_{air} + H(\phi)(\rho_{water} + \rho_{air}), \tag{5}$$

$$\mu(\phi) = \mu_{air} + H(\phi)(\mu_{water} + \mu_{air}), \tag{6}$$

where the subscripts *air* and *water* denote values in the respective domain, and H denotes the Heaviside function, effective across a small number of cells ϵ and defined by

$$H(\phi) = \begin{cases} 0 & \text{if } \phi < -\epsilon \\ \frac{1}{2}\left[1 + \frac{\phi}{\varepsilon} + \frac{\sin(\pi\phi/\varepsilon)}{\pi}\right] & \text{if } |\phi| \le \epsilon \\ 1 & \text{if } \phi > \epsilon. \end{cases} \tag{7}$$

In our simulations we take ϵ equal to twice the width of the grid cells.

3. Numerical approach

3.1. Solution of the Navier–Stokes equations

The Navier–Stokes equations (Eq. (2)) are discretised on a staggered grid with p, ρ and μ defined at grid cell centres and the velocity components at cell faces. Time stepping is achieved with the two-step scheme [11], in which pressure acts as a projection operator that projects an arbitrary velocity field into a divergence-free field. Temporal gradients are discretised with a second-order Runge–Kutta Total Variation Diminishing (RK–TVD) scheme.

In discretising the convective term in Eq. (2) it is essential to avoid the introduction of numerical instabilities due to the sharp density gradient at the interface. To ensure stability, we employ a first-order upwinding scheme in the present numerical model. The diffusive term in Eq. (2) is discretised with a second-order central difference. The surface tension term is modelled using the continuum-surface-force approach discussed by Brackbill et al. [3] and added to the governing equations as a source term. A modified delta function is used to express the force at the interface defined as

$$\delta(\phi) = \begin{cases} \frac{1}{2\epsilon}\left[1 + \cos\left(\frac{\pi\phi}{\epsilon}\right)\right] & \text{if } |\phi| < \epsilon \\ 0 & \text{otherwise} \end{cases} \tag{8}$$

over the same distance ϵ as defined for the Heaviside function above. The unit normal vector $N_i(\phi)$ and the curvature $\kappa(\phi)$ can be computed directly from the grid where

$$N_i = (n_x, n_y, n_z)^T = \frac{\nabla\phi}{|\nabla\phi|}, \tag{9}$$

$$\kappa = \nabla \cdot N_i = n_{x,x} + n_{y,y} + n_{z,z}. \tag{10}$$

We follow a MAC-like discretisation [3] of the surface curvature, in which the components of the normal vector are computed at the cell faces and the curvature follows from taking its divergence.

We use a dynamics time step in which the CFL number is limited by convective, diffusive, gravity and surface tension as discussed by Kang et al. [9]. Here the CFL number is maintained to be equal to 0.5 and the time step Δt is calculated by

$$\Delta t = 0.5\left(\frac{C_{cfl} + \sqrt{(C_{cfl})^2 + 4(G_{cfl}) + 4(S_{cfl})^2}}{2}\right)^{-1}, \tag{11}$$

where $C_{cfl} = \max(|u|/\Delta x, |v|/\Delta y, |w|/\Delta z)$, $G_{cfl} = g/\Delta y$ and Δx, Δy, Δz are the grid increments in the x-, y- and z-directions respectively and $S_{cfl} = \sqrt{\frac{\sigma|\kappa|}{\rho_{air}(\min(\Delta x, \Delta y, \Delta z))^2}}$.

3.2. Solution of the level set equation

Accurate solution of the level set equation (Eq. (1)) is crucial to capture the correct surface physics. Here, we discretise ϕ at cell centres and calculate velocity gradients with a fifth-order HJ–WENO scheme [8]. Temporal gradients are resolved with a third-order TVD Runge–Kutta scheme, see Shu and Osher [20] for details. The same fifth-order HJ–WENO scheme and third-order TVD Runge–Kutta scheme were also used in Enright et al. [4] to evolve the level set equation. Since only the location of the interface is of interest to us, we follow the localisation method of Peng et al. [18] and solve ϕ in a narrow band close to the interface. For the HJ–WENO scheme the narrow band occupies six cell widths either side of the interface in all directions [18].

3.2.1. Reinitialisation of the level set function

As ϕ is evolved in time its distribution throughout the domain may deviate from being a signed distance function (i.e. $|\nabla\phi| \neq 1$) requiring reinitialisation. Here, we reinitialise ϕ, with an efficient fast marching technique at every time step, see Sethian [19] for details. Whilst performing a reinitialisation step, we must specify the value of ϕ at each cell centre that is adjacent to the surface interface which we refer to here as surface cells. In the Hybrid Particle Level Set (HPLS) simulations, this task is effectively performed by the marker particles during the correction phase and thus the value of ϕ at surface cells is anchored during reinitialisation. However, in the absence of marker particles i.e. for level set only simulations, we reinitialise ϕ at surface cells by the particle method proposed by Losasso et al. [15]. This method requires that a massless particle be initialised at each surface cell. Using the surrounding distribution of ϕ the particle is propagated in the normal direction towards the surface a distance equal to the current value of ϕ at the surface grid point. At its new location, an updated value of ϕ is interpolated and the procedure is repeated until the particle lies within a tolerance of the zero interface $\phi < 0.1\Delta x$. The distance from the cell centre to the final resting location of the particle gives the value of ϕ at the surface cell. If the particle does not converge to the surface (i.e. in areas of under-resolved flow) we use linear interpolation between neighbouring cross surface cells to estimate the location of the surface interface and update ϕ accordingly.

3.3. Hybrid Particle Level Set (HPLS) method

To improve the mass conversation properties of the level set method we follow Enright et al. [4] and use a Hybrid Particle Level Set (HPLS) technique in which the distribution of ϕ adjacent to the surface interface is corrected with the aid of massless marker particles. The marker particles are initialised in cells which are less than $1.5\Delta x$ from the surface interface and are advected by the local velocity field by

$$\frac{d\mathbf{x}_p}{dt} = \mathbf{u}(\mathbf{x}_p). \tag{12}$$

Here the velocity $\mathbf{u}(\mathbf{x}_p)$ at the particle location $\mathbf{x}_p$ is determined from the surrounding grid points by trilinear interpolation. We use a third-order accurate TVD Runge–Kutta method to integrate the particles forward in time.

Each particle has a radius r_p which represents its distance from the surface interface and is defined by

$$r_p = \begin{cases} r_{max} & \text{if } s_p\phi(\mathbf{x}_p) > r_{max} \\ s_p\phi(\mathbf{x}_p) & \text{if } r_{min} \leq s_p\phi(\mathbf{x}_p) \leq r_{max} \\ r_{min} & \text{if } s_p\phi(\mathbf{x}_p) < r_{min}, \end{cases} \tag{13}$$

where $s_p = 1$ or -1 dependent upon whether the particle was initially seeded in the positive or negative domains (referred to as positive and negative particles respectively). Here, we set r_{min} and r_{max} equal to $0.05\Delta x$ and $0.5\Delta x$. We are able to parametrise r_{min} lower than the $0.1\Delta x$ suggested by Gaudlitz and Adams [7], due to the improved HPLS technique detailed below.

It is desirable to initialise particles with a random distribution in both the normal and tangential directions with respect to the surface interface. This is achieved by initially placing particles at random locations within cells that are close enough ($<1.5\Delta x$) to the surface interface. Each particle is assigned a goal value of $\phi = \phi_{goal}$ at random and 'attracted' in the normal direction relative to the surface interface until it lies on the desired contour of ϕ, see Enright et al. [4] for more details. Here we make one amendment to their procedure and enforce a minimum surface displacement at initialisation such that $|\phi_{goal}| \geq r_{min}$ and $|\phi_{goal}| \leq r_{max}$. This extra constraint ensures that the radial extent of the particle properly represents the location of the surface interface.

3.3.1. Correction of the level set function

The particles are advected in a separate operation after the level set function has been marched forwards in time. After advection, it is possible to correct the value of ϕ in grid cells that are adjacent to the surface interface. Following the original method of Enright et al. [4], areas of the flow in which the interface representation becomes inaccurate are identified by particles that 'escape' through the interface to the opposite signed domain by more than their radius. An 'escaped' particle p can be used to correct the level set value at the surrounding cell corners $\mathbf{x}_c$ by

$$\phi_p(\mathbf{x}_c) = s_p\big(r_p - |\mathbf{x}_c - \mathbf{x}_p|\big). \tag{14}$$

Since multiple particles may escape in a given cell, each particle's correction is compared against the prospective corrections of all of the other particles that are of the same sign. The prospective positive particle corrections are stored in a variable ϕ^+, where

$$\phi^+ = \max\big(\phi_p, \phi^+\big). \tag{15}$$

Similarly, negative particle corrections are stored in a variable ϕ^-, where

$$\phi^- = \min\big(\phi_p, \phi^-\big). \tag{16}$$

Prior to the correction algorithm $\phi^+ = \phi^- = \phi$.

Finally, after all of the escaped particles have been identified and ϕ^+ and ϕ^- have been constructed the final correction at each grid node is selected by choosing the value with the minimum magnitude,

$$\phi = \begin{cases} \phi^+ & \text{if } |\phi^+| \le |\phi^-| \\ \phi^- & \text{if } |\phi^+| > |\phi^-|. \end{cases} \tag{17}$$

Recently Wang et al. [24] noted that Enright's correction procedure does not allow particles to update cell corners that have the same sign, unless the particle overlapped the corner. We adopt their improved algorithm in which the prospective correction given by positive particles is defined by

$$\phi_p(\mathbf{x}) = \begin{cases} s_p(r_p - |\mathbf{x} - \mathbf{x}_p|) & \text{if } \phi(\mathbf{x}) \le 0 \\ s_p(r_p + |\mathbf{x} - \mathbf{x}_p|) & \text{if } \phi(\mathbf{x}) > 0. \end{cases} \tag{18}$$

Likewise the prospective negative correction is modified to

$$\phi_p(\mathbf{x}) = \begin{cases} s_p(r_p - |\mathbf{x} - \mathbf{x}_p|) & \text{if } \phi(\mathbf{x}) > 0 \\ s_p(r_p + |\mathbf{x} - \mathbf{x}_p|) & \text{if } \phi(\mathbf{x}) \le 0. \end{cases} \tag{19}$$

An additional procedure is carried out to assess the suitability of prospective corrections at each of the grid nodes of cells that contain escaped particles. A projection is made from the grid node along the normal direction of ϕ. The length of the projection is equal to the spacing from the node to the nearest point on the particles surface. If the projected point lies within the grid cell that contained the particle the node is eligible for a correction, see Wang et al. [24] for further details. Rather than updating ϕ in grid cells that contain only 'escaped' particles, an improvement in both accuracy and smoothness can be achieved if all of the surface cells are corrected by the particles contained within. Here, a surface cell is defined as containing either both positive and negative particles or escaped particles. Note, when following this broadband approach to updating ϕ in surface cells it is necessary to initialise ϕ^+ and ϕ^- with large negative and positive values respectively to guarantee that every particle has the potential to update the node.

3.3.2. Improved reseeding method

Despite the improvements in accuracy and smoothness achieved by the method of Wang et al. [24] a potential source of error still arises due to the need to reseed the flow at discrete time intervals. Reseeding is necessary to maintain resolution of the surface interface during stretching, pinching off and merging, but also improves computational efficiency by removing particles that have strayed too far from the surface to aid its capture. During a reseeding operation it is common to specify upper and lower bounds, which define the acceptable number of particles that can occupy a grid cell. When either bound is exceeded, sufficient particles are added or deleted to return the particle density within the cell to it's initial value. If particles are to be deleted from a cell, they are first sorted into order of distance from the surface interface and those that are furthest away are preferentially erased. Particles that have 'escaped' into the opposite signed domain are not deleted irrespective of their number within the cell, since they contain important information with which the surface interface will hopefully be rebuilt at later time steps. Likewise, cells which possess fewer particles than the lower bound our augmented with new particles. The new particles are attracted to a random tangential and normal location (see Section 3.3 above) except the value of ϕ_{goal} is selected to lie within the maximum and minimum nodal values at the cell corners. This strategy works well if the local distribution of ϕ is accurately resolved. However if ϕ is under-resolved locally, the procedure can place particles on the wrong side of the surface interface, see Section 4.1 for evidence of this. Since escaped particles are not deleted the misplaced particles persist there onwards degrading the representation of the surface.

To alleviate this problem, we place an additional operation in the particle reseeding algorithm. The ideology behind our new routine is that in under-resolved regions of the flow, it is the existing particles that give a more accurate representation

of the true interface position than the local distribution of ϕ. We therefore use the location of existing particles to aid the reseeding of new ones. The new particle reseeding strategy is achieved in three steps. Firstly as before, the number of particles is summated in each grid cell and particles are deleted from cells that exceed the maximum threshold or are too far from the interface. Next, in each cell that requires additional particles an attraction phase is used to achieve a random distribution of potential new particles. Finally, each new particle is tested to ensure that it does not overlap any existing particles that are of opposite sign. Since the radial extent of existing particles represents the position of the surface interface, overlapping between opposite signed particles is an indication of misplacement. Overlapping is prevented by calculating the displacement l between the new particle and each pre-existing opposite signed particle that occupies both the same cell and neighbouring cells as well. If l is always greater than the sum of the radius of the new particle and each opposite signed particle radius the placement is acceptable. However, if l is less than the sum of the two radii for any of the opposite signed particles, there is an overlap and the potential new particle is discarded so as not to interfere with the representation of the surface interface. No attempt is made to try to reinitialise discarded particles to maintain the computational efficiency of the algorithm. We refer to this amendment of the standard HPLS method as the non-overlapping concept. Although simple in it's implementation, this extra procedure is shown in Section 4 to significantly improve the accuracy of the Hybrid Particle Level Set method.

Unless stated explicitly below we designate the optimum number of particles per cell $N_p = 32$ and 64 for two-dimensional and three-dimensional simulations respectively. If the number of particles in a cell strays below $0.5N_p$ or above $1.5N_p$ we add or subtract enough particles to restore the optimum number of particles in that cell. Since we anchor ϕ in surface cells we are only required to perform one particle correction per time step as the zero level set contour cannot drift during a reinitialisation step. Our algorithm proceeds as follows: 1. Calculate the level set function at time step $t + \Delta t$; 2. Perform a fast marching redistancing procedure to restore ϕ to a signed distance function; 3. Correct the level set distribution at the surface interface with the particles; 4. Perform a fast marching redistancing procedure again to restore ϕ to a signed distance function; 5. Reseed the particle field; 6. Recalculate the particle radii; 7. Calculate the velocity field at the new time step.

4. Level-set-only test cases

4.1. Two-dimensional constrained vortex flow

Perhaps the most challenging two-dimensional benchmark test for a surface capturing algorithm is the shearing flow induced by a constrained vortex introduced by Bell et al. [2]. Here we initialise a circular interface of radius 0.15, centred at $(0.5, 0.75)$ in a computational domain measuring $L_x = L_y = 1.0$ with $N_x = N_y = 128$ grid cells. The circular interface, which separates the inner negative from the outer positive domain of ϕ, is subjected to a time dependent velocity field given by

$$u = -\sin^2(\pi x)\sin(2\pi y)\cos(\pi t/T), \tag{20}$$

$$v = \sin^2(\pi y)\sin(2\pi x)\cos(\pi t/T), \tag{21}$$

where $T = 8$ s is the total time period of the computation. The cosine term ensures that the constrained field is reversed at $t = T/2$ and the surface interface returns to its circular profile and origin at time $t = T$. We assess the importance of the particle reseeding algorithm through comparison of the original reseeding method of Enright et al. [4], the proposed correction of Wang et al. [24] and our new method with the non-overlapping concept, which we refer to as cases A, B and C respectively. Our error in solving Eq. (12) for the displacement of particles is small ($O(\Delta t)^3$). Therefore the particles return very closely to their initial starting locations giving a model solution with which to compare the accuracy of the reseeding algorithms against. For each test case we consider three different particle densities of 16, 24 and 32 particles per cell and reseed the particles at every time step.

At time $t = T/2$ the initially circular profile is stretched into a thin coiled filament with a long tail; as shown in Figs. 1(a) and 1(b) for the cases A and C respectively. The results shown in Fig. 1(a) are produced by the original reseeding scheme of Enright et al. [4], whereas Fig. 1(b) includes the non-overlapping concept, discussed in Section 3.3.2. The two HPLS algorithms in Figs. 1(a) and 1(b) feature a target particle density of 24 particles per cell and differ only in the method in which particles are reseeded into the flow to maintain resolution of the surface interface. Stretching of the negative domain reduces the thickness of the tail region ($y < 0.2$) and it becomes thinner than the grid spacing. In such regions the construction of the level set function adjacent to the surface interface relies entirely on the correction of the particles, since the gradients of the grid based level set function in Eq. (1) cannot be resolved. The slenderness of the tail causes the negative (interior) domain to become disjointed, forming small blobs of fluid as shown in Figs. 1(c) and 1(d), which are magnified views of the area that is highlighted by green squares in Figs. 1(a) and 1(b) respectively.

The disjointed level set contour occurs whenever the negative particles pass through the centre region of a grid cell without touching any of its grid nodes, where the level set function is defined. In such cells the presence of the negative domain bares no trace in the level set function. If the addition of particles is required in such cells, owing to the particle density falling below the minimum threshold, there is potential for positive particles to be seeded within the negative domain. This is due to the attraction of each newly seeded particle to a random location within the cell using the local level set distribution as a guide to advect the particle to a goal position. Such misplacements of particles are evident in Fig. 1(c)

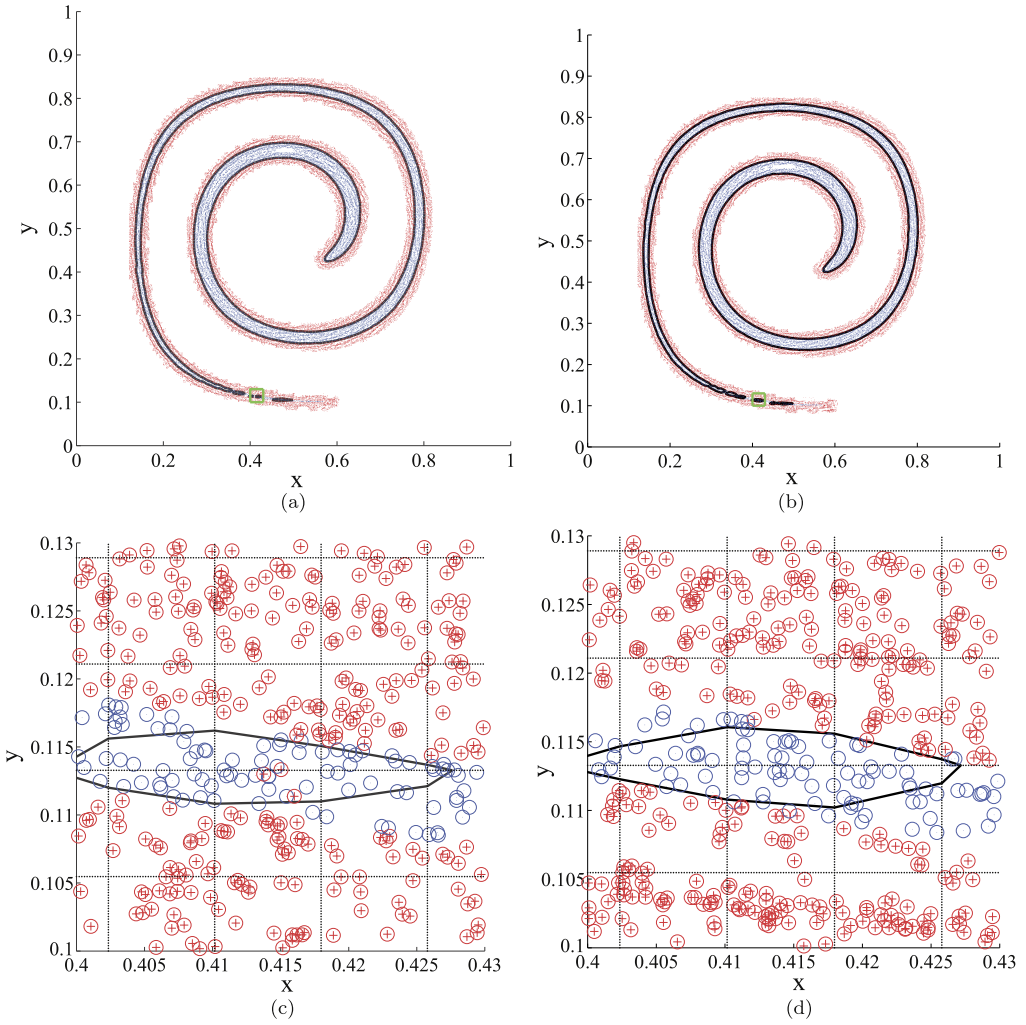

Fig. 1. Zero interface and particle positions for the constrained vortex test case at time $t = T/2$. The results of test case A, which featuring the standard HPLS method of Enright et al. [4], are shown in subfigures (a) and (c). Subfigures (b) and (d) show the results of test case C, in which the non-overlapping concept is employed. Subfigures (c) and (d) show a magnified view of the regions that are highlighted by green rectangles in figures (a) and (b) respectively. Note that the particle radii shown here are not scaled to the actual radius of the particle to aid the clarity of the figure. (For interpretation of the references to color in this figure legend, the reader is referred to the web version of this article.)

where three positive particles are occupying locations within the negative domain, surrounded by negative particles. These positive particles were misplaced at some time prior to the snapshot of the particle field but since they currently have 'escaped' status, occupying a position within the negative domain, they cannot be deleted during a reseeding operation. The deletion of 'escaped' particles is prevented during a reseeding operation to avoid the loss of important information with regard to the location of the zero level set. However, for the corresponding case C (Figs. 1(b) and 1(d)) such a detrimental misplacement of particles has been avoided by the enforcement of the non-overlapping concept.

At later times, as the velocity field reverses and the tail region thickens again, the persistence of misplaced particles in the wrong domain can cause disruption to the smoothness and position of the zero level set contour. An example of this is shown in Figs. 2(a) and 2(b) which document the final location of the zero level set contour for cases A and B. The upper region of the negative domain corresponds to the final resting place of the tail and the location of the misplaced particles. In Wang et al. [24], although their algorithm used a higher-order method to reinitialise the level set function, improving the calculation of the gradients of ϕ used during the attraction of newly reseeded particles, they too showed a similar error in the upper portion at time $t = T$ as seen in Fig. 2(b). The misplacement of particles can also be seen on close inspection of Fig. 5(b) in Wang et al. [24]. Case C, in which the non-overlapping concept is enforced, yields a very close fit with the initially circular level set distribution; see Fig. 2(c). The non-overlapping concept prevents the misplacement of particles throughout the entirety of the simulation improving the accuracy of the HPLS method.

The accuracy of each case can be assessed by computing the loss in area experienced by the negative domain. We calculate the contribution of partially filled grid cells, i.e. those that have both positive and negative values of ϕ at grid

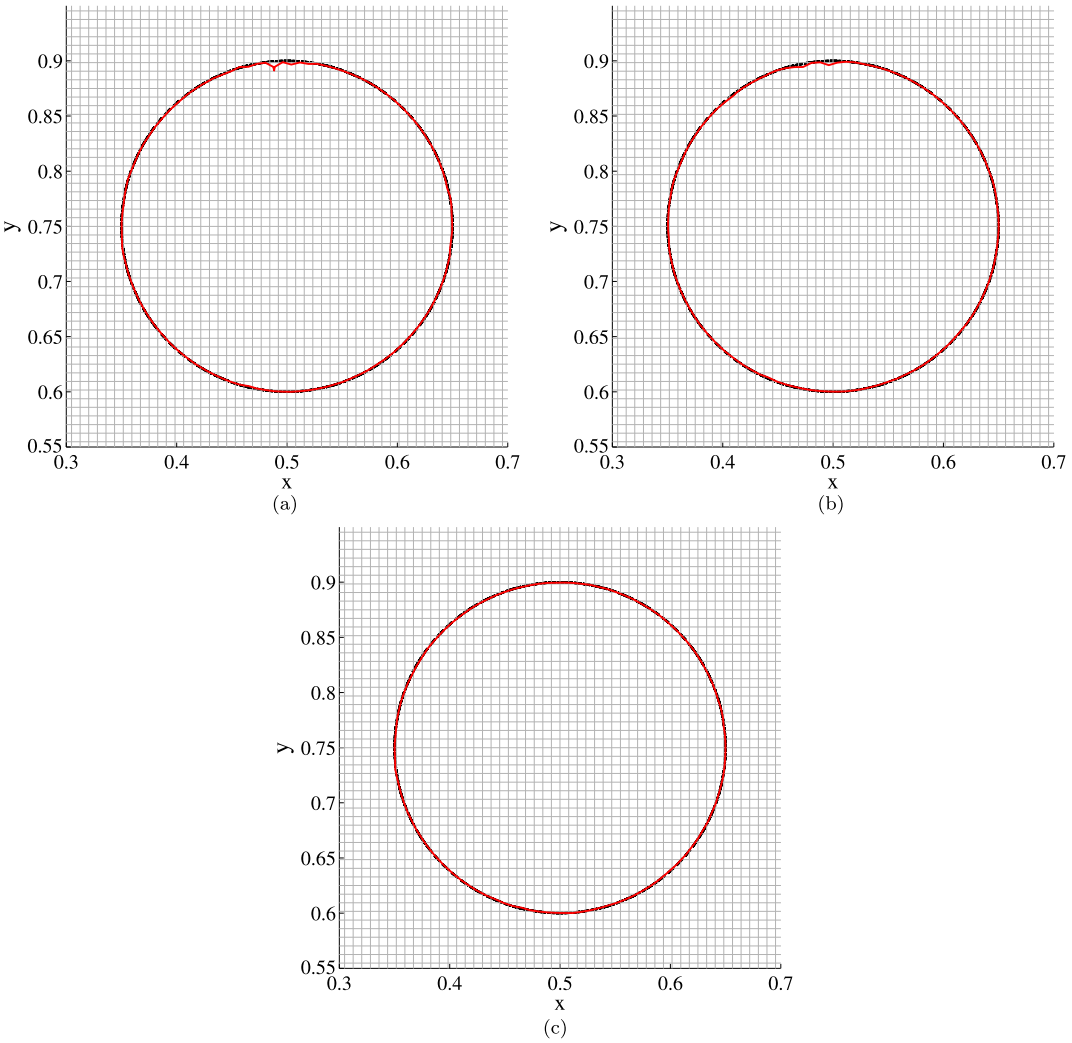

Fig. 2. Final location of the zero level set contour (red solid line) plotted over the initial circular profile (black dashed line) at time $t = T$ for case A (a), case B (b) and case C (c). A density of 24 particles per cell is used for the simulations. (For interpretation of the references to color in this figure legend, the reader is referred to the web version of this article.)

nodes, by subdividing into a 1000 sub-cells. Cubic interpolation is used to calculate the value of ϕ at each sub-cell and the resultant area is added to that of the fully filled cells. Another statistic that reveals the accuracy of the computation is the statistical measure L_1. We follow Sussman and Fatemi [21] and define L_1 as the difference between the actual and computed values of the level set function,

$$L_1 = \sum_{i=1}^{n} \left| \phi_i^{compute} - \phi_i^{actual} \right| / n. \tag{22}$$

The summation is made across the number of cells n that are adjacent to the zero interface. Also of interest is the number of particles that lie on the wrong side of the zero interface by more than their radius ('escaped particles') at $t = T$. In order to compare the geometrical fidelity of the methods, we test the direction of the normal of ϕ at time $t = T$. An angular error is defined as the difference between the analytical solution and the direction of the normal of ϕ in surface cells. Both the maximum and average errors were evaluated in each cell that contained the zero interface. Since all the cases use random number generators to seed and reseed the particles there is scope for a small degree of variability in results. Therefore each simulation is repeated 20 times and the average of these performance measures is recorded in Table 1.

Case C performs better than cases A and B for all particle densities considered as the non-overlapping concept reduces the number of particles that are misplaced during the reseeding process. As one might expect, an increase in the particle density improves the accuracy of the solution for each test case as a better representation of the surface interface is generated. For our non-overlapping concept an increase in particle density also reduces the free space within each cell that

Table 1
Comparison of the performance of reseeding schemes and particle density for the constrained vortex test case. Statistical measures area averaged over 20 runs.

Reseeding scheme	Particles per cell	Area loss %	L_1 error	Number of escaped particles	Maximum angle error	Averaged angle error
A	16	0.52	0.00052	9.55	43.35	3.16
A	24	0.41	0.00036	2.45	26.02	2.23
A	32	0.31	0.00027	1.10	18.98	2.00
B	16	0.49	0.00051	8.30	45.11	3.01
B	24	0.38	0.00036	3.65	35.11	2.19
B	32	0.28	0.00027	0.85	23.35	2.09
C	16	0.33	0.00031	1.65	25.35	1.88
C	24	0.26	0.00023	0.05	14.06	1.59
C	32	0.22	0.00020	0.00	13.78	1.67
AC	24	3.82	0.00517	48.05	87.65	9.50
BC	24	0.90	0.00086	8.90	42.19	3.67
CC	24	0.82	0.00064	1.60	22.14	2.63

is not occupied by either positive or negative particles. If new particles are placed in these gaps, they will pass the non-overlapping criteria but may still not have been placed correctly. Therefore, increasing the particle density improves the ability of the non-overlapping concept to prevent the misplacement of particles. Indeed, only 1 particle was misplaced in 20 repetitions of the test case, when a density of 24 particles per cell was enforced and no particles were misplaced for the highest particle density considered.

The improvement to the HPLS method from the addition of our non-overlapping concept is demonstrated even more dramatically on coarser grids. The final three rows in Table 1 show the results of simulations of the different HPLS methods on a coarser grid with 72 cells in both the x- and y-directions. The statistical measures show that the accuracy of case CC, in which the non-overlapping concept is used on the coarse grid, is significantly higher than both AC and BC (cases A and B on the same coarse grid). In fact, the coarse solution of the case CC is also of similar quality to the solution of cases A and B on the higher resolution grid.

In our future simulations of multi-phase flow, Section 5, we adopt a particle density of 32. This increase in particle density increases the computational time spent by the running of the particle algorithm, however since this is very small ($\ll 1\%$) compared to the time required by the Poisson solver for multi-phase flow, the reduction in overall computational efficiency is negligible and outweighed by the improved accuracy.

4.2. Three-dimensional deformation flow

The performance of our new reseeding algorithm in three-dimensional flows is assessed with the deformation test case used in Enright et al. [4]. Here the velocity field is given by

$$u = 2\sin^2(\pi x)\sin(2\pi y)\sin(2\pi z)\cos(\pi t/T), \tag{23}$$

$$v = -\sin(2\pi x)\sin^2(\pi y)\sin(2\pi z)\cos(\pi t/T), \tag{24}$$

$$w = -\sin(2\pi x)\sin(2\pi y)\sin^2(\pi z)\cos(\pi t/T), \tag{25}$$

and the time period of the simulation $T = 3$ s. The interior of the sphere is represented by negative values of the level set function.

We again contrast the performance of our new reseeding technique with the HPLS methods of Enright et al. [4] and Wang et al. [24], keeping the same case tags as above. A comparison of our improved HPLS technique with the non-overlapping concept (case C) and the HPLS method of Enright et al. (case A) is shown in Fig. 3. Although the deformation of both cases is similar, it is noticeable that case A suffers greater mass loss at $t = T/2$. At this time, the negative domain is stretched to the point where its minimum thickness is less than the grid spacing. This is the period when the simulations are most at risk of particles being misplaced during a reseeding procedure. Evidence that case A suffers more from the misplacement of particles at this juncture is evidenced in the disjointed interface that ensues in the central region of the negative domain; see Fig. 3(a). Misplacement during reseeding can lead to a jumble of positive and negative particles. The level set function in this region will be corrected to a positive or negative value dependent upon which particle is closest to the grid nodes.

A comparison of the final area and performance measures of the three cases are shown in Table 2. Just as in Section 4.1 we repeat the test cases 20 times and display the average measures. For our three-dimensional test case, we again see that far less particles are misplaced by our new method with the non-overlapping concept (case C). In fact only one particle was misplaced in 20 repetitions of the simulation. Cases B and C both out perform the original HPLS of Enright et al. [4], but there is little to separate these cases in the final volume and L_1 measures. Case B, with the Wang et al. correction, performs comparatively better than in the two dimensional test case because of the lower number of misplaced particles.

We selected these two specific benchmark test cases as they present the most extreme challenge to level set methods as one domain becomes stretched thinner than the grid spacing and simulations using level set methods without particles

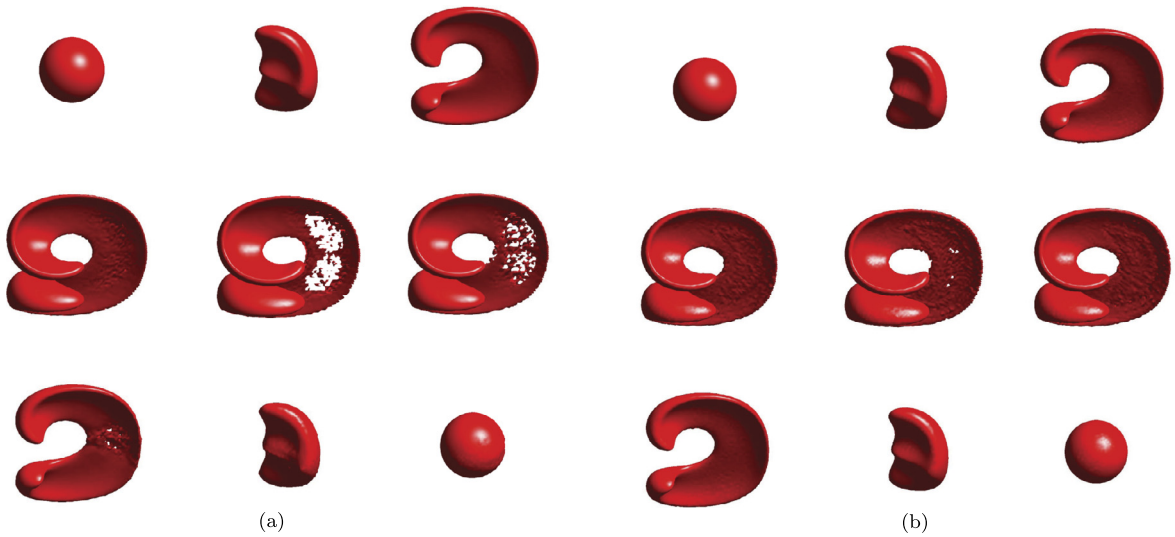

Fig. 3. Three-dimensional deformation test case for method of Enright et al. [4] (a) and our improved HPLS with the non-overlapping concept (b) at $t = 0.0, 0.4, 0.8, 1.2, 1.5, 1.8, 2.2, 2.6$ and 3.0 respectively.

Table 2
Comparison of the performance of reseeding schemes for the three-dimensional deformation test case. Statistical measures area averaged over 20 runs.

Reseeding scheme	Volume loss %	L_1 error	Number of escaped particles
A	2.120	0.001768	29.30
B	1.094	0.000561	2.10
C	1.103	0.000560	0.05

or conservation enforcing algorithms are heavily under-resolved. Despite these challenges the HPLS technique with our additional restriction to prevent the overlapping of particles during reseeding improves the conservation properties of current HPLS methods. This is achieved by preventing particles from being placed in the opposite domain during reseeding, noting that such particles will not be deleted during future reseeding as their status will always be 'escaped' and so can damage the level set profile locally. Although we have used the severe policy of reseeding every time step to present the toughest possible challenge, one can usually relax the spacing between sequential reseeding operations and maintain the same accuracy. Reducing the number of reseeding operations reduces the computational cost of the HPLS method.

5. Two-phase Navier–Stokes flows

In this section we demonstrate the ability of our improved HPLS technique utilising the non-overlapping concept to capture complicated surface dynamics in various benchmark test cases. Unless otherwise stated the reseeding algorithm is performed at every time step. Although this frequency is greater than what is required for the highest computational efficiency, it demonstrates the robustness of our technique.

5.1. Bubble rise

We first consider the rise of a two-dimensional gas bubble in a quiescent liquid in which surface tension plays an important role. The physical parameters chosen for our test case match those used by Gaudlitz and Adams [7] and Wang et al. [24], which although under-resolved, allow for direct comparison with their results. Here the governing equations are non-dimensionalised leading to the introduction of a flow Reynolds number $Re = \rho_l LU/\mu_l = 58$, Froude number $Fr = U/\sqrt{gL} = 1$ and Webber number $We = \rho_l LU^2/\sigma = 104$, where subscript l denotes the physical property in the liquid phase, L and U denote reference length and velocity respectively. The computational domain measures $L_x = 2.5$ and $L_y = 5.0$ and is discretised by $N_x = 40$ and $N_y = 80$ grid cells in the x- and y-directions respectively. The bubble which has a non-dimensional bubble diameter $D_g = 1.0$ is initially centred at $(1.25, 1.25)$ and the simulation is run for 5.0 non-dimensional time units. Finally the ratio of physical parameters of the gas to liquid phases is $\rho_g/\rho_l = 0.025$ and $\mu_g/\mu_l = 0.012$, where subscript g denotes the physical property in the gas phase.

The bubble experiences severe geometric changes during its ascent, shown in Fig. 4. As the bubble rises it initially forms a crescent shape. The diameter of the bubble increases as the crescent arms become thinner and appear to pinch off into two small bubbles. In fact the arms persist as two very thin tails connecting the large parent bubble with the two smaller

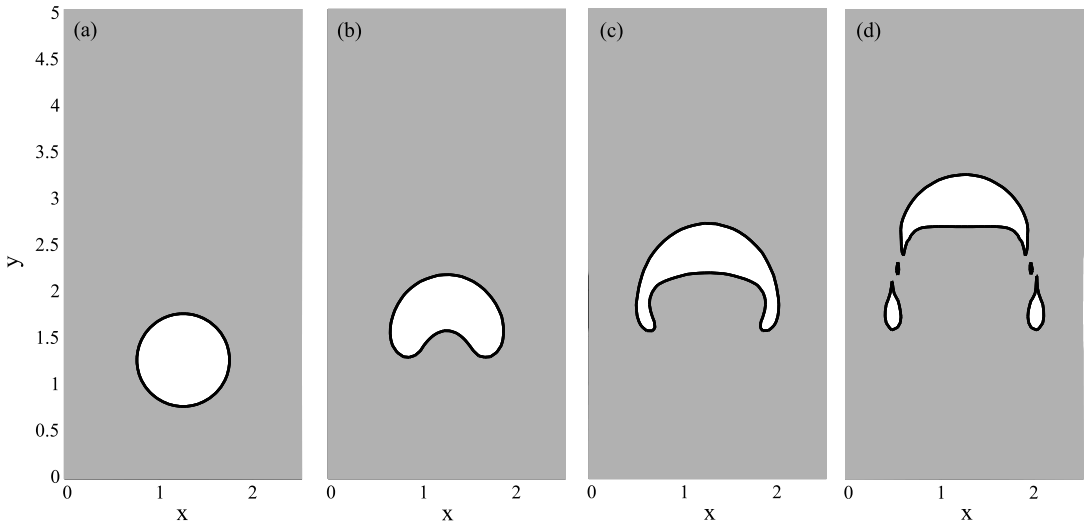

Fig. 4. Bubble rise in a quiescent fluid at times 0.0 (a), 1.5 (b), 3.0 (c) and 4.5 (d). Shaded area denotes liquid phase.

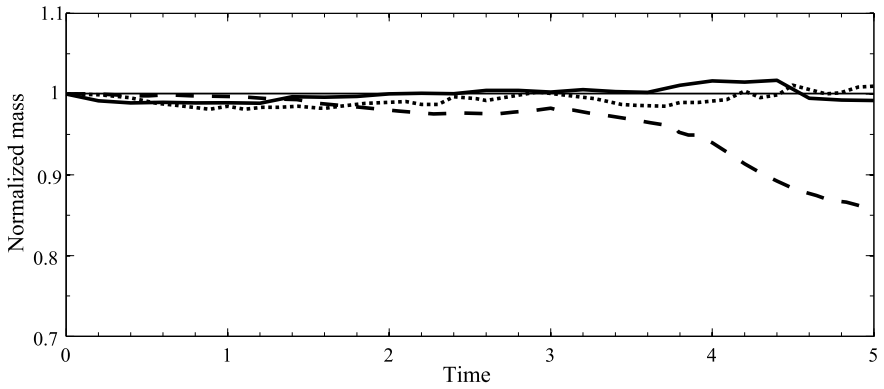

Fig. 5. Comparison of conservation of the volume of water between the new HPLS algorithm (solid line), the particle correction method of Wang et al. [24] (dotted line) and the HPLS method from Gaudlitz and Adams [7] (dashed lines). The horizontal thin solid line represents the analytical solution for comparison.

bubbles behind. When the particles that represent the thin tails pass over the grid nodes, at which the level set function is defined, a number of small blobs of fluid appear. This can be seen in our results as a rise in the overall mass of the air phase in Fig. 5 at approximately time $t = 3.6$ and are evident in the right hand subplot in Fig. 4. At later times, the tails pass away from the grid nodes and the blobs shrink and disappear causing a small decrease in the overall mass of the air phase. Finally at time $t = 5$, the parent bubble forms an oblate-ellipsoidal cap in agreement with the results of Gaudlitz and Adams [7] and Wang et al. [24]. In contrast to the present study and that of Wang et al. [24], Gaudlitz and Adams [7] used the original particle correction of Enright et al. [4]. A comparison of the change in mass of the bubble phase between our present HPLS method and that of Wang et al. [24] and Gaudlitz and Adams [7] is shown in Fig. 5. Despite using a lower-order fast marching method to reinitialise the level set function, our current method performs slightly better than the method of [24] with a maximum error of 1.5% and is far superior to the HPLS method employed by Gaudlitz and Adams [7]. This example demonstrates that although the HPLS method can increase the accuracy of surface tracking greatly, if the smallest details of the surface are important the fineness of the grid must be set accordingly.

5.2. Dam break

The sudden collapse of a water column in a confined tank, known as the dam break test, presents an extreme challenge with which to assess the strengths of our improved HPLS technique. As well as overturning, the fluid also entrains air bubbles and the surface interface undergoes extreme topological changes, high curvature, splitting and merging. The initial fall of the liquid and spreading was recorded experimentally by Martin and Moyce [16] and Koshizuka et al. [13] with the latter authors presenting photographs of the test case. Many authors have used the dam break test case to validate their numerical methods, a recent example of which is Zhang et al. [29].

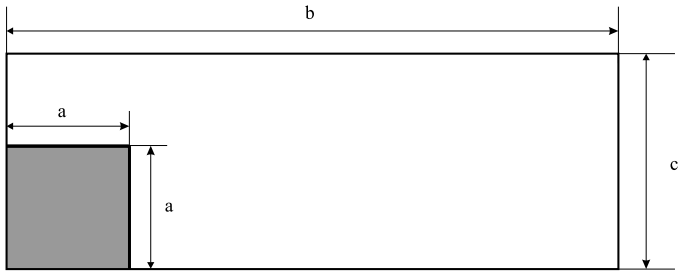

Fig. 6. Schematic diagram of dam break test case.

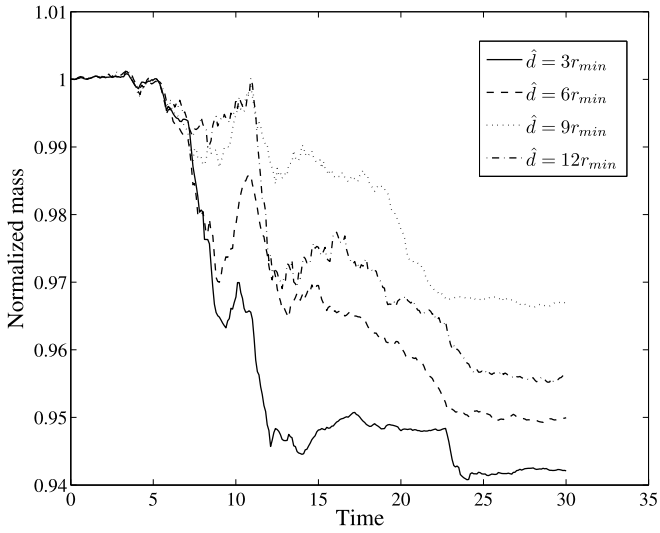

Fig. 7. Comparison of the influence of $\widehat{d}$ on conservation of the volume of water for the new HPLS algorithm.

In order to compare our results directly with the experiments of Martin and Moyce [16], we consider a square column of water with an initial height a within a rectangular domain of length $b = 5a$ and height $c = 1.75a$ (see Fig. 6). The regular Cartesian grid features $N_x = 400$ and $N_y = 140$ cells in the x- and y-directions respectively. The ratio of the liquid density to that of the gas $\rho_l/\rho_g = 830$ and the ratio of dynamic viscosities $\mu_l/\mu_g = 66$. In analysing our results we non-dimensionalise all lengths by a, time t by $\sqrt{a/g}$ and velocities by $\sqrt{ga}$. The relevant non-dimensional parameters for our simulation are Reynolds number $Re = \rho_l U a/\mu_l = 9.98 \times 10^5$, where $U = \sqrt{ga}$ is the reference velocity, Froude number $Fr = U/\sqrt{ga} = 1$ and Webber number $We = \rho_l a U^2/\sigma = 13\,736$. The water column is initially held at rest and then released at time $t = 0.0$.

We have already presented a comparison between the original HPLS method and the experimental data for the fall of water in [1]. Since the same good agreement is achieved with our improved HPLS method we will not repeat the comparison here, but focus on the enhanced mass conservation properties of our new reseeding technique.

The main advantage of our new HPLS algorithm is that by improving particle placement during reseeding operations, far less spurious particles are present to disrupt the simulation. This means that the particle restriction which governs the maximum distance $\widehat{d}$ that a particle can escape without suffering deletion can be increased considerably. An investigation of $\widehat{d}$ is conducted and a comparison of the conservation properties is shown in Fig. 7. Our results show that as $\widehat{d}$ is increased the area conservation properties of our simulation also improve until $\widehat{d} \approx 9r_{min}$, after which the results begin to degrade as the grid and surface representation can no longer cope with the escaped particles. A removal of $\widehat{d}$ is the ultimate goal of our HPLS algorithm, however this is not currently possible for this test case due to the relatively coarse grid and smeared surface. As mentioned above the surface is smeared over a small number of cells with a Heaviside function. When the fluid domain becomes highly stretched the coarsity of the grid and the smeared surface cause the escaped particles to be quickly advected away from the surface. If these escaped particles were not deleted from the simulation they would cause the formulation of spurious blobs of fluid and inhibit merging of overtoppling water, thereby degrading the surface representation. Henceforth we adopt $\widehat{d} = 9.0r_{min}$ in the following calculations for which the maximum change in area remains below 4% in this case even after a long period of simulation. It is noted that in the HPLS method described in [4], the minimum particle radius $r_{min} = 0.1\Delta x$ and limit on escaped particles $\widehat{d} = 1.5r_{min}$. Since in our simulations $r_{min} = 0.05\Delta x$, their results correspond to the present simulation with $\widehat{d} = 3.0r_{min}$. A large escape limit $\widehat{d}$, such as $\widehat{d} = 9.0r_{min}$ recommended here, is not allowed in the original HPLS method of Enright et al. [4], because of the misplacement of particles during reseeding operations, which degrades the surface representation.

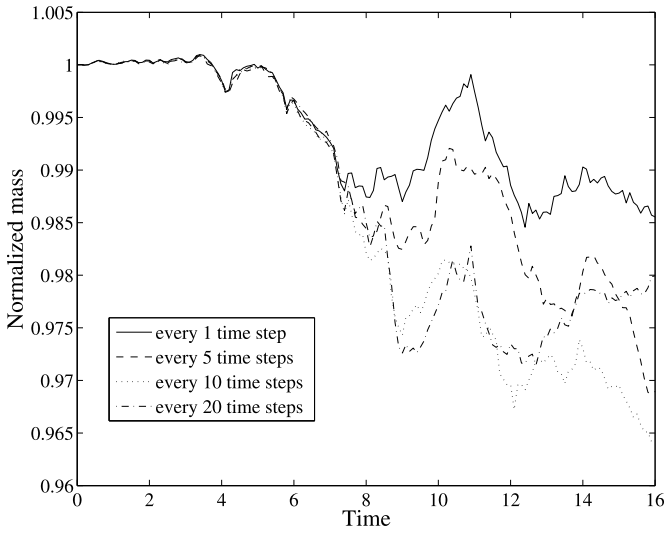

Fig. 8. Comparison of the influence of spacing between reseeding of particles on conservation properties of the new HPLS algorithm.

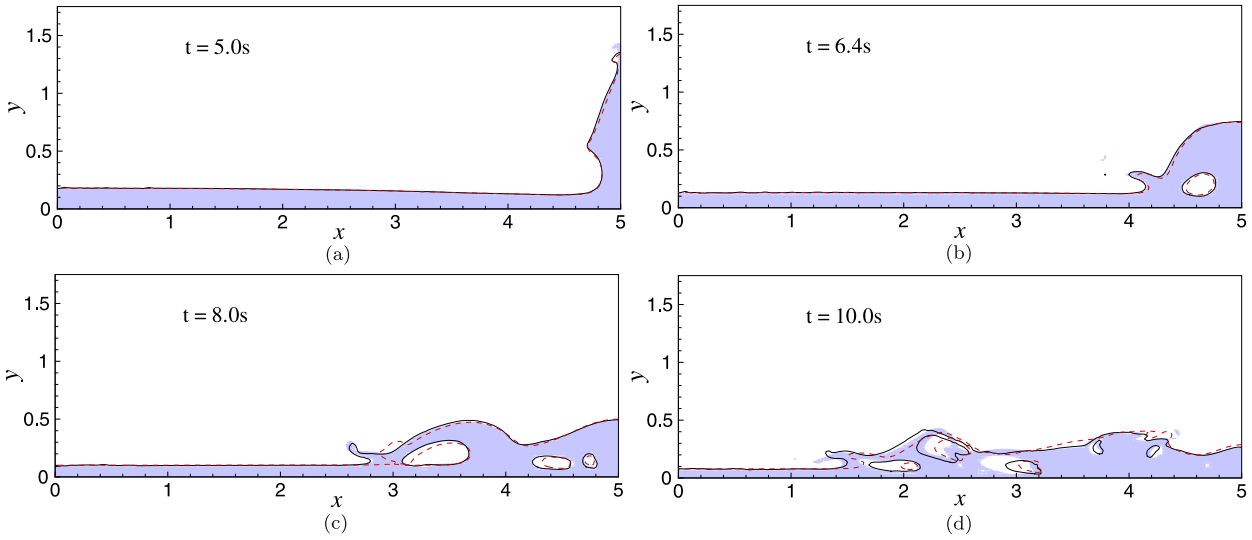

Fig. 9. The water profiles for the dam break test at various times $t = 5.0$ s (a), 6.4 s (b), 8.0 s (c) and 10 s (d) obtained by the LSM without particle corrections (dashed line), the method of Wang et al. [24] (solid line) and the new improved HPLS method (shaded area).

Fig. 8 shows how increasing the spacing between reseeding operations effects the area conservation properties of the new HPLS method. Initially as we increase the spacing from 1–10 time steps the conservation of the fluid phase deteriorates. By reseeding every time step we can maintain at least 16 particles per cell and so maintain good resolution of the interface at all times, which aids the particle reseeding algorithm in placing particles on the correct side of the surface interface.

We now analyse the flow features shown in Fig. 9 to determine how our new HPLS algorithm performs under the rigours of the test case. It should be mentioned that the grid density here is reduced to $N_x = 200$ and $N_y = 70$ cells in the x- and y-directions respectively, in order to better demonstrate the power of the new HPLS method even at a coarse grid. In order to expose the benefits of our new HPLS method (shaded contour) in capturing finer flow features, a direct comparison of the surface interface profile is made with the LSM (dashed line) without particles and the standard HPLS method with the Wang et al. correction method (black line) in Fig. 9. In the case of the standard HPLS method $\widehat{d} = 1.5r_{min}$ and $r_{min} = 0.1\Delta x$ are used to ensure the smoothness of the surface. Whereas in our new non-overlapping HPLS method these parameters are relaxed to $\widehat{d} = 9.0r_{min}$ and $r_{min} = 0.05\Delta x$. Only 78 and 87 minutes of computational time are required to complete the entire 30 s simulation using the LSM without particle corrections and the new HPLS method respectively on a normal workstation with 3 GHz CPU and 12 GB RAM. We can see that our algorithm is efficient, and the introduction of particle corrections does not lead to a significant increase of computer time. A number of higher resolution studies were also undertaken to verify the improvement of the non-overlapping concept. Whilst increasing the resolution reduces numerical diffusion, resulting in

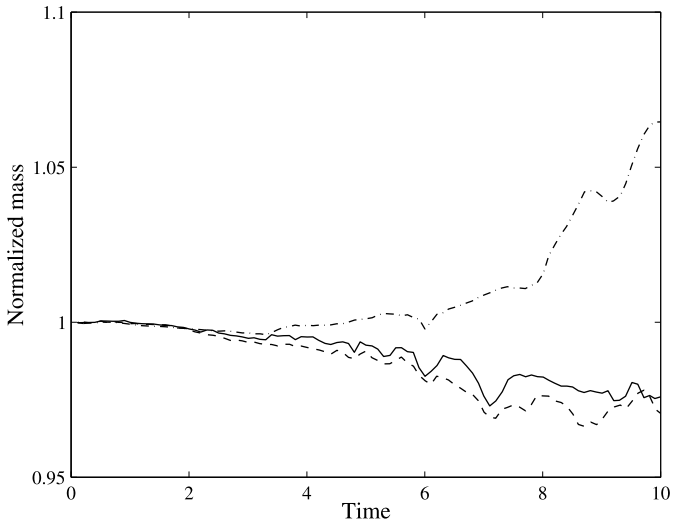

Fig. 10. Comparison of mass conservation properties for the LSM without particle corrections (chain line), the method of Wang et al. [24] (dashed line) and the new improved HPLS method (solid line).

a lower rate of kinetic energy decay in the fluid phase, the large-scale physical behaviour of the water and the benefit of the non-overlapping concept remains unchanged.

Comparison of the water profiles for the different test cases, indicates that all methods capture the surface shape well up to $t = 5.0$ s, at which point the water collides with the dry wall (Fig. 9(a)). During this period, there is no fluid overturning, pinching or merging, indicating that the standard LSM without particle corrections can work well in capturing the interface when the surface curvature is mild. The only noticeable difference is that the new improved HPLS test case propagates further up the right-hand side wall. However, after the overturning wave is generated at $t = 6.4$ s (Fig. 9(b)), the standard LSM (represented by a dashed line in Fig. 9) suffers from regularisation and diffusion in areas of high surface curvature due to its poor mass conservation properties. This results in the shrinking and then loss of the entrained air bubbles that are formed by the overturning waves in Figs. 9 (b) and 9(c), and a corresponding gain in the mass of the fluid phase in Fig. 10. In Fig. 9(b) the first entrained air bubble is formed near the right-hand-side wall and there is good agreement between the three test cases with regard to its shape and size. By $t = 8$ s (Fig. 9(c)) this bubble has collapsed into smaller bubbles, which are then advected towards the surface. At this stage, both HPLS test cases show good agreement in both the size and position of the air bubbles. However, the LSM test case (dashed line) shows a decrease in the bubble size and shape, which is a clear indication of the poorer conservation properties. It is also apparent that the second wave does not travel so far before plunging into the water below for the LSM test case.

Between $t = 8$ s and $t = 10$ s the central bubble in Fig. 9(c) again splinters into two smaller bubbles and the larger of the two breaks through the surface at $x = 4.2$ in Fig. 9(d). For the HPLS test cases, the two remaining bubble artifacts of the first entrained bubble, on the right-hand side of the domain, continue their propagation towards the surface. However, by this point these small bubbles have disappeared from the LSM test case due to diffusion and regularisation of the level set function. By time $t = 10$ s, differences are also apparent between the two HPLS test cases. The non-overlapping concept enhances the conservation properties of our improved HPLS method through relaxation of the distance that a particle can escape without deletion; see Fig. 10. As a consequence less fluid mass is lost and the sloshing and mixing of the air and fluid is more energetic behind the propagating wave front. The wave front has also moved further towards the left-hand side wall for our new improved HPLS test case.

5.3. Impulsive sloshing

We now consider the performance of our numerical method in the simulation of a violent sloshing event in which the surface overturns, splits and merges. A good example of such a situation occurs during the collision of a moving tank with a stationary object. The sloshing is excited by the impulse transmitted to the fluid during the collision. Khezzar et al. [10] performed both experiments and numerical simulations of impulsive sloshing events considering a range of filling ratios and tank accelerations. Their simulations were conducted with the commercial FLUENT package which employs a VOF technique to track the position of the surface. We focus on *Case 2* in their paper in which a tank that measures $182 \times 182 \times 550$ mm is half filled with water. The tank is accelerated from rest at time $t = 0$ in the horizontal (x) direction until it collides with an obstacle at $t = 1.98$ s. The acceleration profile up to the point of impact followed a power law profile, $a(t) = 0.68t^{-0.11}$ and the velocity of the tank at the time of collision measured $u_c = 1.41$ m/s.

Here we idealise the collision in a two-dimensional computation, which is reasonable since the flow pattern in the tank is also approximately two-dimensional. The computational domain consisted of a regular Cartesian grid of 220×70 cells

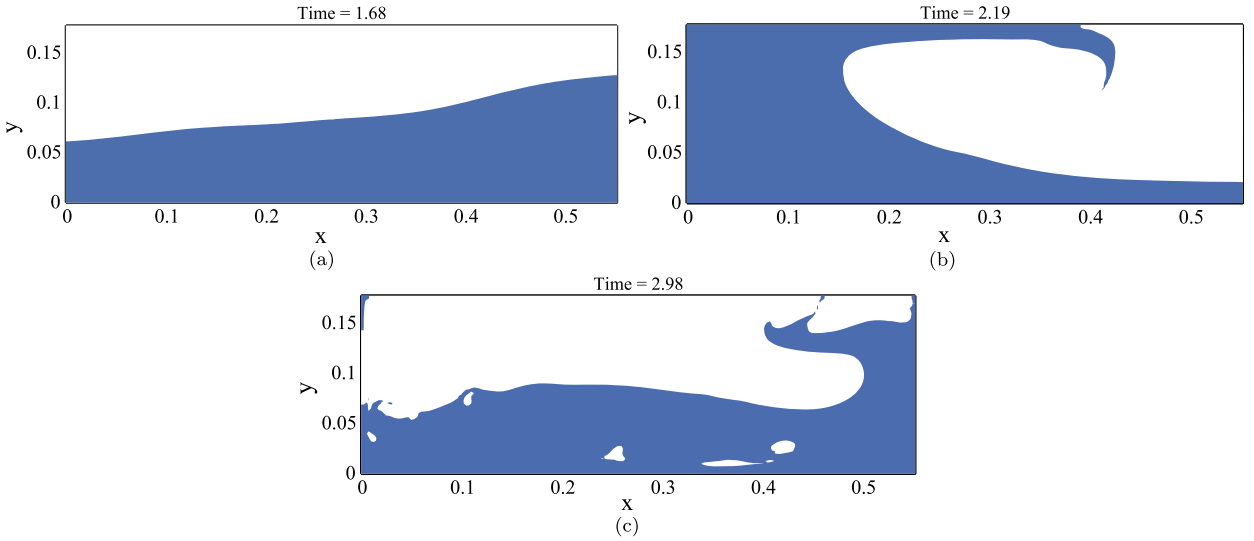

Fig. 11. Location of the water phase at times $t = 1.68$ (a), 2.19 (b) and 2.98(c).

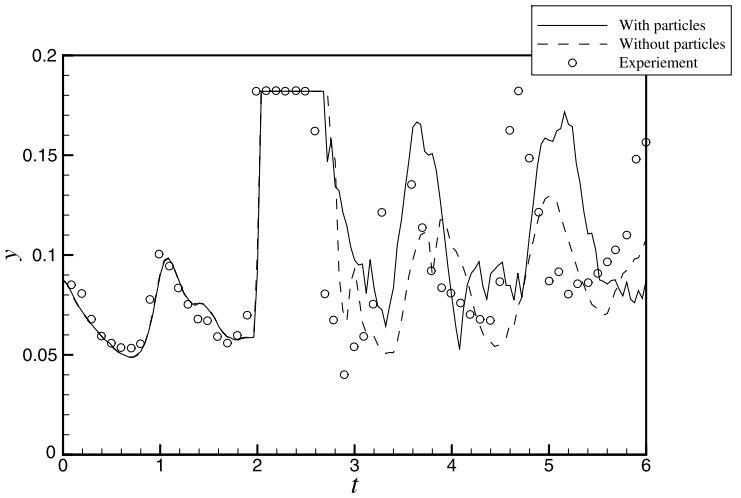

Fig. 12. Comparison of surface displacement η at the left-hand side wall between experiments and the current numerical results.

in the x- and y-directions respectively. During the acceleration phase of the tank motion we model the fluid behaviour in a co-moving reference frame by adding a body force term f_x to the Navier–Stokes equations. The tank accelerates in the negative x-direction to allow for direct comparison with the experiments. At the time of the collision the tank comes to rest instantaneously and thus $f_x = 0$ from this point onwards. To model the impulse on the fluid at the point of impact we follow Khezzar et al. [10] and modify the horizontal velocity to $u - u_c$. The simulation then proceeds in a stationary frame of reference. After the simulation has finished we calculate the dynamic pressure Q along the vertical tank walls.

Prior to the collision at $t < 1.98$ s the tank accelerates from right to left causing fluid to build up in the right-hand side of the tank (see Fig. 11(a)). A surface wave with an approximate amplitude of 0.025 m and wavelength equal to the tank length propagates through the tank evidenced in the surface displacement at the location of the left-hand side wall (see Fig. 12). The wavy behaviour is likely to be caused by the sudden nature of the tank acceleration and is also notable in the experimental results. Immediately after collision, the water moves quickly towards the left-hand wall and overturns much like a plunging ocean wave (Fig. 11(b)). The movement of water away from the right-hand wall towards the left-hand wall causes a marked increase in the dynamic pressure Q, at both walls but approximately twice as large at the left-hand wall (see Figs. 13(a), 13(b)). The overturning water makes contact with the right-hand side wall at time $t = 2.23$ s, which is highlighted with an intense peak in the dynamic pressure in Fig. 13(b). The water then continues to slosh from right to left walls for the remainder of the simulation but inducing far lesser dynamic pressures on the walls.

Throughout our simulation the overall motion of the water agrees well with that of the experiments (see Fig. 12) however some discrepancy exists between the height to which the surface reaches at the left-hand side at time $t \approx 4.8$ s. Certain features are present in the numerical results that are absent from the experimental pictures in [10]. Due to the

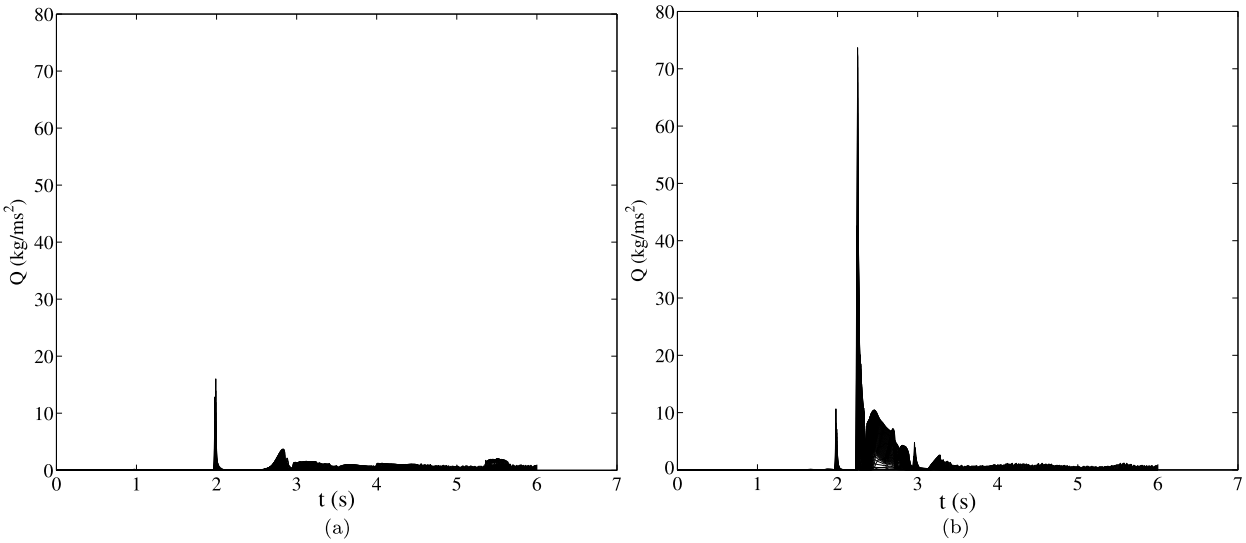

Fig. 13. Dynamic pressure Q at every grid cell along the left- (a) and right-hand side (b) walls of the tank.

two-dimensional nature of our simulations, overturning fluid captures air bubbles below the surface (see Fig. 11(c)). It is possible that such small trapped air bubbles are blended out by the experimental image capturing technique or perhaps that the air escapes in the spanwise direction (not modelled here). It can be also seen in Fig. 11(c) that water becomes trapped in both the upper left and upper right corners of the domain. This is due to the impermeable boundary condition enforced at the top of the domain. Since the amount of fluid trapped at the corners is a very small fraction of the overall volume of fluid it will not influence our results greatly. It is also noted that there would be a small amount of residue fluid droplets present at the upper surface and walls of the tank in the experiments after the fluid has passed across. Fig. 12 also demonstrates the vast improvement of the HPLS method over the standard level set method without the particle correction, which effectively dissipates the energy within the sloshing fluid, preventing it from rising up the tank walls.

6. Conclusion

In this paper we have developed and tested a novel non-overlapping concept to improve both the accuracy and suitability of the HPLS method for the simulation of multi-phase fluid flows. The non-overlapping concept effectively prevents the misplacement of particles during reseeding operations and thereby relaxes the common restriction placed on escaped particles. This restriction involves the deletion of particles which escape to the opposite signed domain by more than $1.5r_{min}$ to maintain the integrity of the surface interface. By implementing our non-overlapping concept we have been able to triple the escape limit of particles and in doing so increased the accuracy of the solution. This has been demonstrated by a number of challenging test cases and an optimisation of the gap between reseeding operations and particle density and size has been performed.

The final goal must be to develop an HPLS technique in which the restriction on escaped particles can be completely removed. At present this is not possible in both the dam break and impulsive sloshing cases recorded herein. It can be speculated that increasing the grid cell density through parallelisation of the existing code and implementation of a sharp surface representation detailed in [26] could achieve this goal and it is hoped that future research will focus on this challenge. In particular the specification of a sharp interface will allow fine fluid particles that are of diameter equal to a small number of grid cells to be more realistically affected by gravity. This would prevent escaped fluid from being quickly convected away in the gas phase due to the high velocities present close to the surface when the liquid overturns. A notable feature is inherent to the blended representation of the surface in our current numerical code.

Acknowledgements

The authors gratefully acknowledge the financial support provided by the Faculty Research Committee (FRC) Grant R-264-000-260-133 at the National University of Singapore. The authors would also like to thank Professor Rodney Eatock Taylor of the University of Oxford and the National University of Singapore for helpful discussions.

References

[1] P. Archer, W. Bai, Applicability of particle level set method for simulation of breaking waves, Int. J. Offshore Polar Eng. 23 (2) (2013) 129–136.
[2] J. Bell, P. Collela, H. Glaz, A second-order projection method for the incompressible Navier–Stokes equations, J. Comput. Phys. 85 (1989) 257–283.

[3] J. Brackbill, D. Kothe, C. Zemach, A continuum method for modeling surface tension, J. Comput. Phys. 100 (1992) 335–354.
[4] D. Enright, R. Fedkiw, J. Ferziger, I. Mitchell, A hybrid particle level set method for improved interface capturing, J. Comput. Phys. 183 (2002) 83–116.
[5] D. Enright, F. Losasso, R. Fedkiw, A fast and accurate semi-Lagrangian particle level set method, Comput. Struct. 83 (2005) 479–490.
[6] D. Enright, D. Nguyen, F. Gibou, R. Fedkiw, Using the particle level set method and a second order accurate pressure boundary condition for free surface flows, in: Proc. 4th ASME–JSME, FEDSME2003–45144, 2003.
[7] D. Gaudlitz, N. Adams, On improving mass-conservation properties of the hybrid particle-level-set method, Comput. Fluids 37 (2008) 1320–1331.
[8] G.-S. Jiang, C.-W. Shu, Weighted ENO schemes for Hamilton–Jacobi equations, SIAM J. Sci. Comput. 21 (2000) 2126–2143.
[9] M. Kang, R. Fedkiw, X.-D. Liu, A boundary condition capturing method for multiphase incompressible flow, J. Sci. Comput. 15 (2000) 323–360.
[10] L. Khezzar, A. Seibi, A. Goharzadeh, Water sloshing in rectangular tanks – an experimental investigation and numerical simulation, Int. J. Eng. 3 (2009) 174–184.
[11] J. Kim, P. Moin, Application of a fractional step method to Navier–Stokes equations, J. Comput. Phys. 59 (1985) 308–323.
[12] M. Kim, J. Park, W. Lee, A new VOF-based numerical scheme for the simulation of fluid flow with free surface. Part II. Application to the cavity filling and sloshing problems, Int. J. Numer. Methods Fluids 42 (2003) 791–812.
[13] S. Koshizuka, H. Tamako, Y. Oka, A particle method for incompressible viscous flow with fluid fragmentation, Comput. Fluid Dyn. J. 113 (1995) 134–147.
[14] D. Liu, P. Lin, A numerical study of three-dimensional liquid sloshing in tanks, J. Comput. Phys. 227 (2008) 3921–3939.
[15] F. Losasso, R. Fedkiw, S. Osher, Spatially adaptive techniques for level set methods and incompressible flow, Comput. Fluids 35 (2006) 995–1010.
[16] J. Martin, W. Moyce, An experimental study of the collapse of liquid columns on a rigid horizontal plate, Philos. Trans. R. Soc. Lond. A 244 (1952) 312–324.
[17] S. Osher, R. Fedkiw, Level set methods: an overview and some recent results, J. Comput. Phys. 169 (2001) 463–502.
[18] D. Peng, B. Merriman, S. Osher, H.-K. Zhao, M. Kang, A PDE based fast local level set method, J. Comput. Phys. 155 (1999) 410–438.
[19] J. Sethian, A fast marching level set method for monotonically advancing fronts, Proc. Natl. Acad. Sci. USA 93 (1996) 1591–1595.
[20] C.-W. Shu, S. Osher, Efficient implementation of essentially non-oscillatory shock-capturing schemes, J. Comput. Phys. 77 (1988) 439–471.
[21] M. Sussman, E. Fatemi, An efficient interface-preserving level set redistancing algorithm and its application to interfacial incompressible fluid flow, SIAM J. Sci. Comput. 20 (1999) 1165–1191.
[22] M. Sussman, E. Puckett, A coupled level set and volume-of-fluid method for computating 3D and axisymmetric incompressible two-phase flows, J. Comput. Phys. 162 (2000) 301–337.
[23] G. Tryggvason, B. Bunner, A. Esmaeeli, D. Juric, N. Al-Rawahi, W. Tauber, J. Han, S. Nas, Y.-J. Jan, A front-tracking method for the computations of multiphase flow, J. Comput. Phys. 169 (2001) 708–759.
[24] W. Wang, J. Yang, F. Stern, An improved particle correction procedure for the particle level set method, J. Comput. Phys. 228 (2009) 5819–5837.
[25] Y. Wang, S. Simakhina, M. Sussman, A hybrid level set-volume constraint method for incompressible two-phase flow, J. Comput. Phys. 231 (2012) 6438–6471.
[26] J. Yang, F. Stern, Sharp interface immersed-boundary/level-set method for wave-body interactions, J. Comput. Phys. 228 (2009) 6590–6616.
[27] Y. Yap, J. Chai, K. Toh, T. Wong, Modeling the flows of two immiscible fluids in a three-dimensional square channel using the level-set method, Numer. Heat Transf., Part A, Appl. 49 (2006) 893–904.
[28] W. Yue, L. Ching-Long, V. Patel, Numerical simulation of unsteady multidimensional free surface motions by level set method, Int. J. Numer. Methods Fluids 42 (2003) 853–884.
[29] Y. Zhang, Q. Zou, D. Greaves, Numerical simulation of free-surface flow using the level-set method with global mass correction, Int. J. Numer. Methods Fluids 63 (2010) 651–680.